

Deposition of SnO₂ buffer layer onto commercial conducting glass to be used in thin films solar cells technology

S. Melo, E. Rodríguez

Centro de Investigación en Ciencia Aplicada y Tecnología Avanzada, Unidad Altamira - Instituto Politécnico Nacional, Altamira, Tamps., 89600, México.

O. Vigil Galán

Escuela Superior de Física y Matemáticas-Instituto Politécnico Nacional (IPN), Gustavo A. Madero, CDMX, 07738, México.

C. A. Hernández-Gutiérrez*

Departamento de Física, CINVESTAV-IPN, México, Gustavo A. Madero, CDMX, 07360, México.

F.A. Pulgarín-Agudelo

CONACYT-Escuela Superior de Física y Matemáticas-Instituto Politécnico Nacional, Benito Juárez, CDMX, 03940, México.

H. Mendoza-León

Centro de Nanociencias y Micro y Nanotecnologías-Instituto Politécnico Nacional (IPN), Gustavo A. Madero, CDMX, 07738, México.

(Submitted: October 18th, 2017; Accepted: December 10th, 2017)

In this work the influence of the deposition of SnO₂ buffer layer on the optical, electrical and morphological properties of commercial conducting glasses is presented. Previously the transparent conducting oxide (TCO) were studied in order to determine which is the most appropriate in solar cell applications. The SnO₂ thin films were deposited onto glass and commercial conducting glass by pneumatic spray pyrolysis (PSP) and magnetron sputtering techniques and characterized optically and electrically. TCO/buffer bi-layers configuration were processed and characterized through a modified well-known Haccke figure of merit. The results are discussed in terms of considering the usefulness or otherwise of this configuration, depending on the morphological quality of commercial conductive glass in the processing of second-generation solar cells in thin film technology.

Introduction

SnO₂ has been the most widely used metal oxide in applications such as gas sensor [1,2], and solar cells [3,4]. In particular in the thin film solar cells with superstrate configuration, the SnO₂ has been used as buffer layer between the TCO and CdS in particular where the CdTe is used as active compound-absorber [5,6]. SnO₂ have been implemented for interface passivation in SnS solar cells. Recombination near the p-SnS/n-Zn(O,S) junction is reduced by inserting a few monolayers of SnO₂ between these layers [7]. Recently SnO₂ thin film has been used like intermediate layer at Cu₂ZnSnS₄/CdS interface, studying the interface defect passivation in kesterite thin film solar cells [8]. Sb₂Se₃, a promising alternative light absorber for photovoltaic application is a new absorber material used in solar cells with superstrate configuration [9-11] and also a strate configuration has been designed in Sb₂Se₃ solar cell, analogous to CIGS-structure [12]. In both applications only, fluorine-doped tin oxide (FTO) has been used as TCO, therefore the inclusion of a SnO₂ buffer layer in this new type of solar cell in the superstrate configuration in an open research. SnO₂ has been deposited by different techniques as

successive ionic layer adsorption and reaction (SILAR), sputtering, spray pyrolysis, chemical vapor deposition and atomic layer deposition (ALD) [13-17]. Due to its stronger mechanical and chemical stability at high temperature, together with the relative abundance of Sn makes this metal oxide one of the most used with different type of dopants. On the other hand, generally many research groups acquire commercial conductive glasses and others synthesize them to be used as TCO in the processing of solar cells, In the first case the commercial conducting glasses with SnO₂:F as TCO, are manufactured for more generic uses than polycrystalline thin film solar cells processing purposes and therefore not always have the suitable morphological properties for this specific use [18]. In this reference, it was clearly demonstrated how a TCO of pessimism morphological quality, completely degrades the properties of the solar cell, using it in the manufacturing process. A buffer layer of SnO₂ deposited on a FTO contributes to improve its morphological properties (decrease in the number of pinholes and the roughness), especially if the TCO presents a poor quality in this parameter. To improve this aspect, it has been considered the use of a FTO/SnO₂ bilayer as an alternative to the use of a simple TCO as front contact in

* chernandez@fis.cinvestav.mx

solar cells processed in the superstrate configuration, where the SnO₂ is an intermediate layer between the TCO and the so-called window material, which is usually the CdS.

The PSP technique, is a low-cost and simple method, which has been used during the last three decades, as one of the major techniques to deposit SnO₂ thin films, whereas, magnetron sputtering is a mature technique that allows to obtain SnO₂ thin films with great reproducibility and good physical properties. In the reference [18] the use of the TCO/buffer layer combination with the thermal treatment on the CdS/CdTe solar properties was studied, showing a reduction of the specific front contact resistance (from 4.72 to 0.4 Ω·cm²), which means a reduction on the series resistance and the improvement of the solar cell efficiency from 4.1 to 11%.

Considering the aforementioned aspects, two objectives have been proposed in this work. To study the properties of two commercial glass that are traditionally used in the processing of solar cells, but which, until our knowledge, are selected arbitrarily. And to evaluate the two methods that are traditionally used in the deposits of thin films of SnO₂ used as buffer layer. It is necessary to clarify that the study carried out in this work, not only is applied to the use of a bi-layer TCO/buffer, but also to the use of the SnO₂ as high resistive layer (HRL). The importance of band alignment using HRL layers has been studied with different oxides as buffer layers [19-21]. The band alignment means a reduction in the energy barrier at the interface TCO/semiconductor, which is beneficial for the transfer and collection of the charge carriers in solar cells and reduces the minority carrier recombination at the interface.

Experimental details

In the first step T-7 (7 Ω/sq and 0.38 μm) and T-15 (15 Ω/sq and 0.35 μm) commercial conducting glasses (TEC GLASS, Pilkington) were selected for study their properties as TCO. The properties of a TCO are evaluated commonly by the well-known figure of merit of Haacke [22]:

$$F. M. = \frac{(T_{ave})^{10}}{R_{sh}} \quad (1)$$

Where T_{ave} is the average transmittance and R_{sh} is the sheet resistance. This figure of merit only considers the optical and electrical properties of the TCO, however is not sufficient for the use of a TCO in applications related to solar cells, because it does not consider its morphological properties. In order to overcome this limitation, we have defined a modified Haacke's figure of merit as:

$$F. M. = \frac{(T_{ave})^{10}}{R_{sh}} \frac{1}{R} \quad (2)$$

Where R is the roughness of the sample surface, which is a very important requirement for a substrate on which different thin films are deposited (other parameter like the number of pin-holes are usually in this new type of figure of merit). As has been mentioned before, the manufacture of the commercial conducting glasses is based on optimizing the optical and electrical properties without including the morphological one.

In order to evaluate the figure of merit given in Equation (2), in as-grown and annealed samples, a post-thermal annealing in Ar atmosphere during 30 minutes at 500 °C was carried out. The optical, electrical and morphological properties were studied by using a Perkin Elmer Lambda 35 UV/Vis Spectrometer, a home made four probe equipment, a JEOL scanning electron microscope (SEM) (Model: SEM JSM-7800F). The roughness of the samples was investigated by Atomic Force Microscopy (AFM), employing a Solver Next instrument from NT-MDT. The measurements were carried out in tapping mode and low scanning frequency (0.4 Hz). The AFM measurements were performed for 5 points near the center of each sample, to establish an average roughness with scan areas of 30×30 μm².

Once the commercial conductive glass has been selected, according to the previous study, SnO₂ buffer-layers were deposited onto glass substrate by PSP and magnetron sputtering techniques. For the PSP deposition, SnCl₄·H₂O dissolved in a mixture of ethanol and deionized water (1:1) was sprayed onto glass substrates. The distance between the nozzle and the sample was 30 cm, 40 kPa and 5 ml/min were used as gas pressure and solution flow, respectively and substrate temperature was established at 570 °C. Samples were deposited on areas of 6.25 cm². For this deposition technique, an automatic spray system was used [23], in which the speed of movement of the nozzle was varied in a range of 4-30 cm/min, taking the heighted speed according to the experimental results (not shown). For the deposition of SnO₂ thin films via RF magnetron sputtering, the pure SnO₂ target was used and the substrate-to-target distance was 30 cm. The chamber of magnetron sputtering was evacuated to a base pressure of 1×10⁻³ Pa before the deposition. The sputtering power under Ar atmosphere was 80 W, the deposition time of 50 minutes and the working pressure of 2.7 Pa were maintained constant for all depositions. Both the samples deposited onto glass substrate by pneumatic spray pyrolysis (PSP) and by sputtering were submitted to a thermal post-treatment at 400 °C during 45 minutes under O₂ atmosphere. The objective of this treatment is to introduce oxygen atoms in the layer to compensate the vacancies of this element in the compound and increase its resistivity.

Finally, SnO₂ thin films were deposited onto the as-grown and annealed conducting glass substrate and the TCO/SnO₂ bi-layers were divided into two substructures: one with the as-grown SnO₂ layer and the other ones with the SnO₂ layer annealed in O₂ atmosphere under the same conditions explained above. In this way, the as-grown and annealed conducting glass substrate, the as-grown and annealed SnO₂ layers and the combined as-grown-annealed conducting glass substrate/SnO₂ stack have been studied.

Results and discussion

Characterization of commercial conducting glass

In Figure 1 the transmittance spectra of the commercial conductive glasses are shown. As can be seen from this Figure, two aspects are relevant for these commercial conductive glasses: (a) T15 has a higher transmittance than T7, which is derived from the lower thickness. As known,

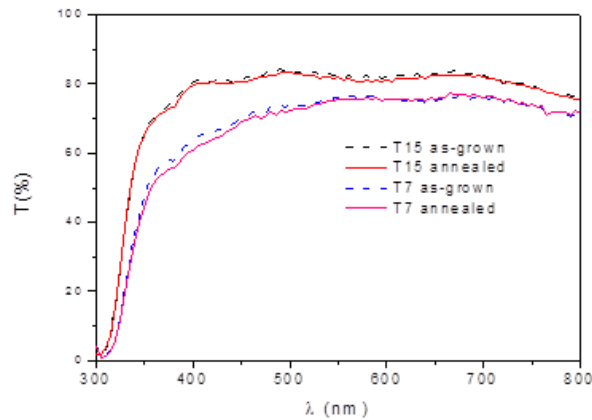


Figure 1. Optical transmittance spectra of the commercial conducting glasses T-7 and T-15: as-grown (dash lines) and annealed in Ar atmosphere (solid lines).

$T \sim \exp(-\alpha d)$, where α is the absorption coefficient and d the thickness. On the other hand, the sheet resistance varies with the inverse of the thickness ($R_{sh} = \rho/d$).

A TCO with a sheet resistance of $7 \Omega/\text{sq}$. is thicker than a TCO of $15 \Omega/\text{sq}$. Therefore it will have a smaller transmittance, in correspondence with Figure 1, the thermal treatment does not substantially change the transmittance with respect to the as-grown samples. A band gap value of 3.76 eV was estimated from the derivative of these spectra. The surface morphology of T-7 and T-15 via SEM images is shown in Figure 2.

Larger grain sizes are observed in the as-grown T-7 sample, with respect to those of T-15. The measured thickness of the T-7 was higher than that of T-15 (0.38 and $0.35 \mu\text{m}$, respectively). Larger grain sizes may explain lower resistivity of T-7 than T-15, due to the fact that a lower amount of grain boundaries. The grain sizes do not change substantially with the post-thermal annealing in Ar atmosphere, confirming the results of optical transmission shown in Figure 1.

Table 1 shows the influence of the post thermal annealing in Ar atmosphere on the electrical, optical and morphological properties of the T-7 and T-15. Both, Haacke's figure of merit and the modified one give maximum values for the thermal annealed samples, with higher value corresponding

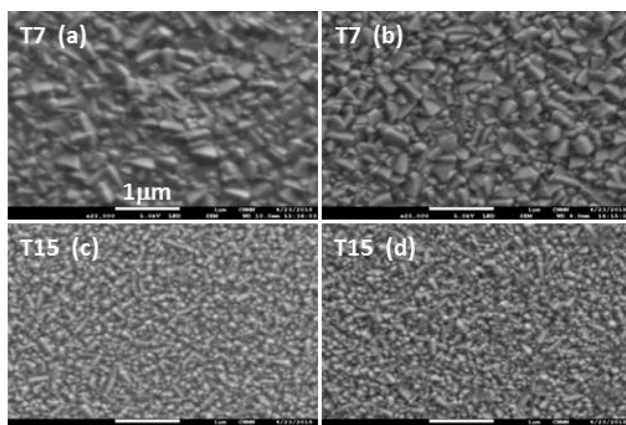


Figure 2. SEM images of T-7 and T-15 commercial conducting glasses: (a) and (c) as grown samples, (b) and (d) annealed samples.

Table 1. Comparison of sheet resistance (R_{sh}), average transmittance (T_{ave}) and roughness (R) expressed through Haacke's and Haacke's modified figures of merit and band-gap value (E_G) of as-grown and thermal annealed in Ar atmosphere of commercial conducting glass. (The values shown in the table were averaged in five samples in each case).

Commercial conducting glass	R_{sh} (Ω/sq)	T_{ave} (%)	R (nm)	T^{10}/R_{sh} (Ω^{-1}) $\times 10^{-3}$	$(T^{10}/R_{sh}) \cdot 1/R$ ($\Omega^{-1}\text{nm}^{-1}$) $\times 10^{-5}$	E_G (eV)
T-7-asgrown	7.8	64.6	20.2	1.6	8	3.8
T-7 annealed	8.6	64.0	19.8	1.3	7	3.8
T-15-asgrown	15.0	75.9	17.2	4.2	24	3.9
T-15 annealed	14.9	74.0	9.2	4.0	40	3.9

to T15, which means that this TCO is optimized with respect to T7 in its optical, electrical and morphological properties.

From the results shown in Table I it concludes that the T-15 is more appropriate to be used as TCO in the processing of solar cells than the T-7, and therefore this TCO was chosen as a substrate in the following processes.

Characterization of SnO₂ thin films

A buffer layer must have the following properties: (a) highly resistive to eliminate as much as possible the interdiffusion, through it, between the atoms of the adjacent layers; (b) of the smallest possible thickness to reduce its incidence on the series resistance of the device; and (c) a high transmittance. Taking into account the above, we have defined the following figure of merit for buffer layers:

$$(R_{sh} T_{ave}^{10})/d \tag{3}$$

The maximum value of this figure of merit optimizes the three mentioned aspects. Figure 3 shows the transmittance spectra of the SnO₂ buffer layers after the thermal annealing. Table 2 summarizes the values of the sheet resistance, average transmittance, thickness, resistivity and the corresponding figure of merit of as-grown and annealed SnO₂ samples deposited by PSP and magnetron sputtering techniques on the glass substrates.

The sheet resistance of the films deposited by PSP is higher than those deposited by sputtering in all cases. These results can be explained as follows: In the PSP method the formation of the compound SnO₂ is the result of the reaction

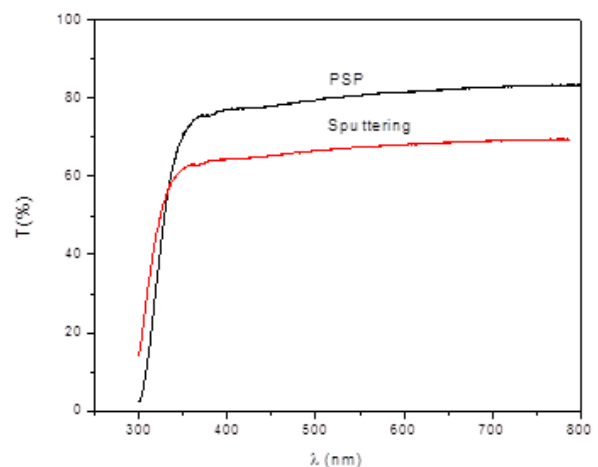


Figure 3. Optical transmittance spectra of the annealed SnO₂ thin films.

Table 2. Sheet resistance (R_{sh}), average transmittance (T_{ave}), thickness (d) and resistivity (ρ) values of as-grown and annealed SnO_2 layers deposited onto glass substrate by PSP and magnetron sputtering techniques.

SnO_2 deposition	R_{sh} (Ω/sq) $\times 10^3$	T_{ave} (%)	d (nm)	ρ ($\Omega.cm$)	$R_{sh}\cdot T_{ave}^{10}/d$ (Ω/nm) $\times 10^6$
PSP as-grown	1000	75.8	17	1.76	3.7
PSP annealed	1100	76.3	17	1.76	4.3
Sputt. as-grown	31.7	67.6	35	0.09	0.02
Sputt. annealed	70.0	64.4	31	0.2	0.02

between the Sn from the salt with the oxygen of the surrounding air in the growth chamber (the carrier gas used in these deposits is air). The reaction between a salt containing Sn and oxygen using air as a carrier gas in the PSP technique is well known, such that the SnO_2 samples grown by this technique are characterized by growing in an oxygen rich environment. A different situation occurs in the sputtering depositions, where the properties of the SnO_2 thin films depend on the stoichiometry of the target, the conditions of the environment inside the chamber and the deposit parameters.

In our experimental conditions the deposition is made under Ar atmosphere in the chamber and therefore the oxygen content in the film depends on the stoichiometry of the target and the loss of this element in the deposition process. Reactive sputtering with a flow of oxygen is usually introduced in the chamber to control of oxygen content in the sample [20,21]. Oxygen vacancies give the n-type conductivity character to the SnO_2 compound, because the vacancies of oxygen cause that the tin yields its electrons to the crystalline structure. An increase in the number of oxygen vacancies determines an increase in conductivity. In general, thin films with a higher oxygen content should be obtained when the PSP technique is used, respect to the sputtering ones and therefore more resistive samples, as shown in table II. Following the same reasoning, the thermal annealing should not have significant effect on the electrical

properties of films deposited by PSP, while in the case of the sample deposited by sputtering the same thermal annealing in oxygen atmosphere is more effective and therefore an increase in the shunt resistance and resistivity is obtained. Concluding, resistive SnO_2 films with thickness of 17 nm are obtained by the PSP technique and less resistive with thicknesses of the order of 30 nm by sputtering, which determines that the former better fulfill the properties of buffer layers than the latter, as shows the figure of merit. In the case of films deposited by PSP on a glass substrate, the post-thermal annealing does not change the properties of the films with respect to as-grown one.

Higher average transmittance is obtained in the case of the films deposited by PSP with respect to those deposited by sputtering, due to the thicknesses of the layers and the calculated values of band-gap were approximately the same (4.0 eV). The band-gap varies from 3.54 eV to 4.20 eV according to the values reporting in literature conditions [23,24].

From preliminaries XPS measurements (no shown in this work) the O/Sn ratio value was estimated for layer deposited by PSP and sputtering. The O/Sn ratio value closer to 2 (1.9) for the sample deposited by PSP and 1.65 by sputtering, reveals a more stoichiometry in the case of sample deposited by PSP in comparison with the sputtering ones. It is known that completely stoichiometric SnO_2 is an insulator or at most an ionic conductor. However, in practice this material is never stoichiometric and invariably presents defects, fundamentally oxygen vacancy.

Characterization of conducting glass substrate/ SnO_2 stacking

In order to compare the properties of the TCO/ SnO_2 bilayer with those described above in the case of commercial TCO, we have first calculated the equivalent resistance of the bilayers. From the electrical point of view, these bilayers form a parallel resistance system, in which the total resistance of the system is given by the following relationship:

$$\frac{1}{R_T} = \frac{1}{R_{TCO}} + \frac{1}{R_{buffer}} \Rightarrow R_T = \frac{R_{TCO}R_{buffer}}{R_{TCO}+R_{buffer}} \tag{4}$$

Figure 4 shows the transmittance spectra of the TCO/ SnO_2 structures, where the buffer layers have been deposited by PSP and sputtering techniques. In both cases the T15 and the buffer layers were subjected to the thermal treatments explained above.

Comparing Figures 1 and 4 it is observed that the deposit of the buffer layers, both by PSP and by sputtering on the TCO, does not alter its transmittance, as a consequence of the thicknesses of the buffer layers, significantly lower than the TCO ones. A slight decrease in the thickness of the layers under thermal treatment was observed, probably due to a greater compactness of the grains and a loss of material under this treatment.

The morphological properties obtained from the AFM technique are shown in Figure 5. With the thermal annealing, the film particle of the sample deposited by PSP increases while an opposite process occurs for the sample deposited by

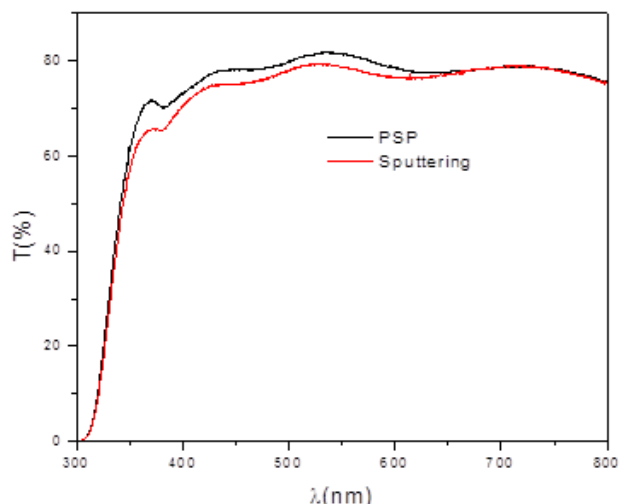


Figure 4. Transmittance spectra of TCO/ SnO_2 structures, where the buffer layer was deposited by PSP and by sputtering.

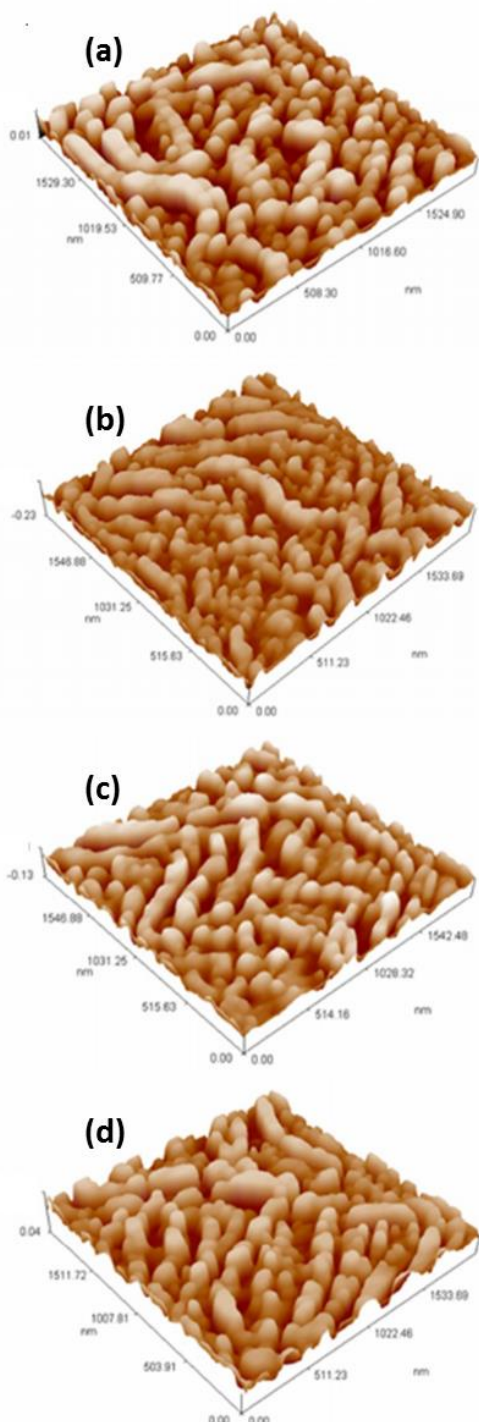


Figure 5. AFM images of samples of TCO/SnO₂ structures: (a) as-grown PSP-SnO₂; (b) annealed PSP-SnO₂; (c) as-grown Sputtering-SnO₂; and (d) annealed Sputtering-SnO₂.

Table 3. Sheet resistance (R_{sh}), average transmittance (T_{ave}), thickness of TCO+SnO₂ layer(d), RMS roughness (R) and Haacke’s modified figure of merit of the TCO/buffer bi-layers. (Only TCO and SnO₂ annealed samples are presented according with the results shown in table II).

T-15/SnO ₂ conditions	R_{sh} (Ω /sq)	T_{ave} (%)	$d_{(TCO+SnO_2)}$ (nm)	R (nm)	$(T^{10}/R_{sh}) \cdot 1/R$ ($\Omega^{-1}nm^{-1}$) $\times 10^{-5}$
SnO ₂ by PSP	14.1	72.9	376	2.1	107
SnO ₂ by Sputtering	15.3	72.5	385	2.8	90

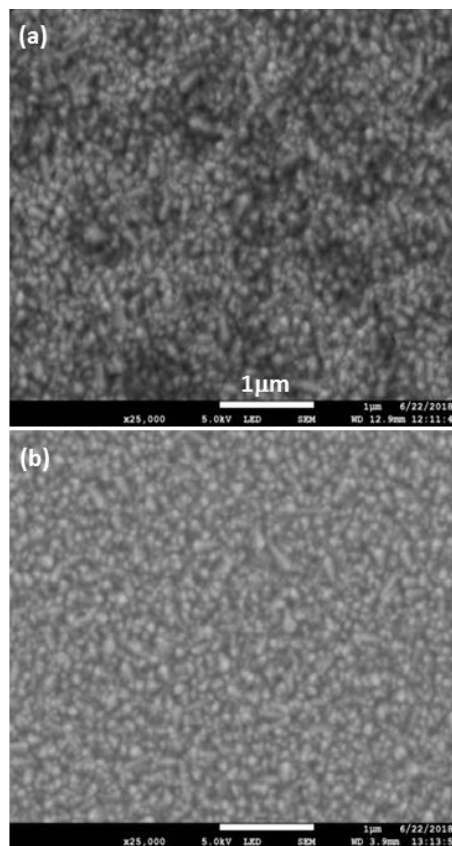


Figure 6. SEM images of TCO/SnO₂ bi-layers annealed, with SnO₂ deposited by: (a) PSP and (b) Sputtering.

sputtering, and the surface roughness was similar for both structures. The post-thermal treatment has a greater effect in reducing the roughness of the structure in the case of the SnO₂ layer deposited by sputtering, respecting that deposited by PSP.

Finally, the calculated values of R_T according with the equation (4) correspond to the measured ones. Table 3 summarizes the values of the shunt resistance, average transmittance, thickness, RMS roughness and Haacke’s modified figure of merit of the TCO/buffer structure.

Figure 6 shows the top view SEM micrographs of the surfaces of the TCO/SnO₂ bi-layers both with post- thermal annealing. A better uniformity is observed in the layer deposited by sputtering on T15 with a better contrast, according with the higher conductivity. Therefore, a better morphological property is obtained when the SnO₂ layer is deposited on the conducting glass substrate T15 by sputtering technique.

Conclusions

Our results show that for photovoltaic applications, commercial conductive glass T15 is better TCO than T7. From the comparison of Tables 1 and 3, the use of the SnO₂ as buffer layer improvement the TCO properties. Moreover, if the morphology is considered, the results of Table 3 show that both the PSP and sputtering techniques are appropriate for the deposition of SnO₂ as buffer-layers in solar cells with superstrate structure. In reference [18] we show that, if a



TCO presents a low morphological quality, the deposit of the buffer layer considerably improves the properties of the TCO and of the solar cells. In this work, we have shown that TCO with good optical, electrical and morphological properties, the deposition of a buffer layer does not produce significant changes in the properties of the TCO. In contrast, with the case of nonhomogeneous TCOs, with many pin-holes and/or high roughness. The results shown in this paper allow an assessment of the type of TCO to be used and its improvement in the processing of high efficiency solar cells in thin film technology.

Acknowledgments

O. Vigil-Galán and E. Rodríguez acknowledge support from COFAA and EDI of IPN. F. Pulgarín acknowledges to the Mexican founding agency Consejo Nacional de Ciencia y Tecnología (CONACyT) under project 183728. The authors acknowledge to Georgina Ramirez-Cruz for her technical support for the AFM measurements. Authors also acknowledge the financial support from National Polytechnic Institute under project SIP.

References

[1]. A.B.F. Martinson, J.W. Elam, J. Liu, M.J. Pellin, T.J. Marks, J.T. Hupp, *Nano Lett.* **8**, 2862 (2008).
 [2]. F. Yang, S.R. Forrest, *Adv. Mater.* **18**, 2018 (2006).
 [3]. A.K. Ghosh, C. Fishman, T. Feng, *J. Appl. Phys.* **49**, 3490 (1978).
 [4]. W. Ke, G. Fang, Q. Liu, L. Xiong, P. Qin, H. Tao, J. Wang, H. Lei, B. Li, J. Wan, G. Yang, Y. Yan, *J. Am. Chem. Soc.* **137**, 6730 (2015).
 [5]. C.S. Ferekides, R. Mamazza, U. Balasubramanian, D.L. Morel, *Thin Solid Films* **480**, 224 (2005).
 [6]. S. Gayam, S. Bapanapalli, H. Zhao, L. Nemani, D.L. Morel, C.S. Ferekides, *Thin Solid Films* **515**, 6060 (2007).

[7] P. Sinsersuksakul, L. Sun, S.W. Lee, H.H. Park, S.B. Kim, C. Yang, R.G. Gordon, *Adv. Energy Mater.* **4**, 1400496 (2014).
 [8] H. Sun, K. Sun, J. Huang, C. Yan, F. Liu, J. Park, A. Pu, J.A. Stride, M.A. Green, X. Hao, *ACS Appl. Energy Mater.* **1**, 154 (2018).
 [9] M. Luo, M. Leng, X. Liu, J. Chen, C. Chen, S. Qin, J. Tang, *Appl. Phys. Lett.* **104**, 173904 (2014).
 [10] Y. Zhou, L. Wang, S. Chen, S. Qin, X. Liu, J. Chen, D.-J. Xue, M. Luo, Y. Cao, Y. Cheng, E.H. Sargent, J. Tang, *Nat. Photonics* **9**, 409 (2015).
 [11] X. Liu, X. Xiao, Y. Yang, D.-J. Xue, D.-B. Li, C. Chen, S. Lu, L. Gao, Y. He, M.C. Beard, G. Wang, S. Chen, J. Tang, *Prog. Photovolt: Res. Appl.* **25**, 861 (2017).
 [12] X. Liu, J. Chen, M. Luo, M. Leng, Z. Xia, Y. Zhou, S. Qin, D.-J. Xue, L. Lv, H. Huang, D. Niu, J. Tang, *ACS Appl. Mater. Interfaces* **6**, 10687 (2014).
 [13] M.A. Yıldırım, S.T. Yıldırım, E.F. Sakar, A. Ateş, *Spectrochim. Acta A: Mol. Biomol. Spectrosc.* **133**, 60 (2014).
 [14] H.-R. Kim, G.-H. Lee, D.-H. Kim, *J. Phys. D Appl. Phys.* **44**, 185203 (2011).
 [15] G. Korotcenkov, V. Brinzari, J. Schwank, M. DiBattista, A. Vasiliev, *Sensors Actuat. B-Chem.* **77**, 244 (2001).
 [16] Y.M. Lu, J. Jiang, M. Becker, B. Kramm, L. Chen, A. Polity, Y.B. He, P.J. Klar, B.K. Meyer, *Vacuum* **122**, 347 (2015).
 [17] H.-E. Cheng, D.-C. Tian, K.-C. Huang, *Procedia Eng.* **36**, 510 (2012).
 [18] O. Vigil Galán, D. Jiménez Olarte, G. Contreras-Puente, M. Courel, *J. Renew. Sustain. Energy* **7**, 013115 (2015).
 [19] A. Klein, *J. Phys.: Condens. Matter* **27**, 134201 (2015).
 [20] J.M. Kephart, R.M. Geisthardt, W.S. Sampath, *Prog. Photovolt. Res. Appl.* **23**, 1484 (2015).
 [21] J.M. Kephart, J.W. McCamy, Z. Ma, A. Ganjoo, F.M. Alamgir, W.S. Sampath, *Sol. Energy Mater. Sol. Cells* **157**, 266 (2016).
 [22] G. Haacke, *J. Appl. Phys.* **47**, 4086 (1976).
 [23] K. Kant, D. Losic, R.E. Sabzi, *Int. J. Nanosci.* **10**, 1 (2011).
 [24] G.E. Patil, D.D. Kajale, S.D. Shinde, V.B. Gaikwad, G.H. Jain, *Int. Nano Lett.* **2**, 46 (2012).

© 2018 by the authors; licensee SMCTSM, Mexico. This article is an open access article distributed under the terms and conditions of the Creative Commons Attribution license (<http://creativecommons.org/licenses/by/4.0/>).